Chinese Physics Letters **42**, 110302 (2025) **Express Letter**

Role of Degenerate States on Molecular Excitation by Intense Laser Pulses

Bo Li(李波)[1†], Yan Rong Liu(刘艳荣)[1†], Victor Kimberg[2], Maomao Gong(宫毛毛)[1], Yongjun Cheng(程勇军)[1], Yong Wu(吴勇)[3,4], Jian Guo Wang(王建国)[3], Jing Chen(陈京)[5], and Song Bin Zhang(张松斌)[1*]

[1]*School of Physics and Information Technology, Shaanxi Normal University, Xi'an 710119, China*
[2]*International Research Center of Spectroscopy and Quantum Chemistry (IRC SQC), Siberian Federal University, 660074 Krasnoyarsk, Russia*
[3]*Institute of Applied Physics and Computational Mathematics, Beijing 100088, China*
[4]*Center for Applied Physics and Technology, Peking University, Beijing 100084, China*
[5]*School of Physical Sciences, University of Science and Technology of China, Hefei 230026, China*

(Received 4 August 2025; accepted manuscript online 8 September 2025)

A singlet diatomic molecule naturally carries doubly degenerate $\pm\Lambda$ states when the projection of the total electronic angular momentum onto the internuclear axis is nonzero. These doubly degenerate states contribute equally in conventional measurements and are thus treated the same in corresponding simulations. In this study, we demonstrate that in resonant excitation by intense laser pulses, the doubly degenerate $\pm\Lambda$ states must be clearly identified. This is exemplified in the $X^1\Sigma \to A^1\Pi$ transition of CO molecules. This distinction becomes especially important in the case of circularly polarized radiation. We attribute this phenomenon to the interference of electron-rotational pathways in the strong-field coupled transition with the $\pm\Lambda$-state of the excited Π state. This research sheds light on the fundamental aspects of intense laser-molecule interactions when extending conventional theories.

DOI: 10.1088/0256-307X/42/11/110302 CSTR: 32039.14.0256-307X.42.11.110302

1. Introduction. In a diatomic molecule, the electronic angular momentum projection along the internuclear axis is represented by Λ. This value classifies molecular states as Σ, Π, Δ, etc. When Λ is nonzero and the molecule is in an electric field, reversing the motion of all electrons maintains the system's energy but interchanges $+\Lambda$ and $-\Lambda$. This results in the doubly degenerate $\pm\Lambda$ states.[1,2] For the one-photon excitation between the $^1\Sigma$ and $^1\Pi$ states, the transition strengths ($\sigma_{\Pi_{\pm\Lambda}\Sigma}$) to the $\Pi_{+\Lambda}$ and $\Pi_{-\Lambda}$ states are equivalent.[3] Consequently, in the weak field limit, the doubly degenerate $\Pi_{+\Lambda}$ and $\Pi_{-\Lambda}$ states are spectrally indistinguishable.

Thanks to the dramatic advancements in ultrashort and intense short-wavelength laser pulses,[4–10] a wide range of theoretical studies have focused on diatomic $X^1\Sigma \to {}^1\Pi$ transitions to explore ultrafast and nonlinear phenomena using ultraviolet (UV) and X-ray pulses.[11–16] The light-induced conical intersection introduces strong nonadiabatic couplings by mixing rotational, vibrational and electronic motions,[17,18] resulting in significant changes in the intense UV photodissociation dynamics.[19–25] The Rabi-cycling of electronic transitions by intense UV pulses can strongly couple the electron-rotation dynamics and change the coupled rovibrational dynamics and spectra.[26–31] In the resonant Auger decay induced by an intense X-ray laser field, the doubly intersecting complex electronic surfaces, arising from nonadiabatic couplings between matrix elements of nuclear vibrational and rotational motions, results in dramatic dynamic effects on the resonant Auger electron spectra.[32–35]

In previous studies using intense laser pulses, researchers have carefully investigated the electron-rotational and vibrational couplings by treating the doubly degenerate $\Pi_{\pm\Lambda}$ states as the same Π state, similar to the way in conventional weak-field. In most studies,[21,32,36–38] the electronic orbital angular momentum is considered "tied" to the internuclear axis,[2] resulting in the angular electronic transition operators depending only on the polar angle β and azimuthal angle α.[39–41]

However, for states with nonzero Λ, the electronic orbital angular momentum can also rotate around the molecular axis, introducing an additional rotational angle γ, as shown in Fig. 1(a) for Hund's case (a) coupling.[2] In our previous works, examining the $X^1\Sigma \to {}^1\Pi$ transitions in diatomics induced by linearly polarized (LP) intense laser fields, we considered the role of γ and highlighted the crucial coupling between the angular moment Λ and the nuclear rotational angular momentum for electronic excitations.[26–31] However, only transitions to the $\Pi_{+\Lambda}$-state were studied, with the expectation that the $\Pi_{-\Lambda}$-state would yield similar results.

In this paper, we consider the interaction with both

†These authors contributed equally to this work.
*Corresponding author. Email: song-bin.zhang@snnu.edu.cn
© 2025 Chinese Physical Society and IOP Publishing Ltd. All rights, including for text and data mining, AI training, and similar technologies, are reserved.

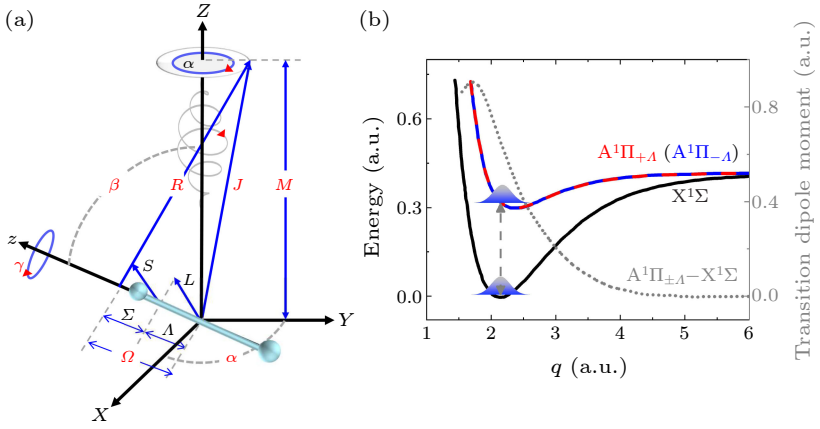

Fig. 1. (a) The various quantities of angular momentum in Hund's case (a) coupling (following Zare [2] notations) and Euler angles ($\alpha\beta\gamma$) with respect to the space-fixed frame (X–Y–Z). Ignoring the angular momentum projection on molecular axis results in $\Lambda = 0$ (or redundant γ) and $J = R$. Circularly polarized laser field propagating along Z-axis is shown schematically by the solid gray line. (b) Potential energy curves for the $X^1\Sigma$ (black) and $A^1\Pi$ (red and blue) states of the CO and the transition dipole moment (dashed gray) are shown. [42,43]

$+\Lambda$ and $-\Lambda$ states in the $X^1\Sigma \to A^1\Pi$ transition, induced by LP and circularly polarized (CP) resonant intense UV pulses in the CO molecule. We demonstrate that the doubly degenerate $\pm\Lambda$ states significantly impact rotational excitations in the $X^1\Sigma$ state, as a result of the coherent suppression of transition channels between $\Pi_{+\Lambda} \to \Sigma$ and $\Pi_{-\Lambda} \to \Sigma$ within the electronic Rabi-cycling induced by the strong UV pulse. This effect is particularly pronounced for CP pulses and can have a substantial influence on rotational populations in high-intensity scenarios. The observed impact of degenerate states on coupled electronic and rovibronic excitations offers new insights into molecular dynamics in the realms of strong-field and ultrafast science. Throughout this paper, atomic units (a.u.) are utilized, unless stated otherwise.

2. Computational Methods. Within the Born–Oppenheimer approximation in Hund's case (a) [Fig. 1(a)], the total wave function $|\varphi\rangle$ for a singlet state may be written as a product of electronic orbital $|\Lambda\rangle$, vibrational $|\nu\rangle$, and rotational $|J, M, \Omega\rangle = (\frac{2J+1}{8\pi^2})^{1/2} D^J_{M,\Omega}(\alpha\beta\gamma)$ parts, so that $|\varphi\rangle = |\Lambda\rangle|\nu\rangle|J, M, \Omega\rangle$. [2] Note that the projection of the total angular momentum J onto the space-fixed Z-axis is M, the total angular momentum about the molecular axis is $\Omega = \Lambda + \Sigma$, where Λ and Σ are the projections of the total orbital angular momentum L and spin angular momentum S onto the molecular axis, respectively. Note that for the studies of singlet states, both S and Σ are zero, and $\Omega = \Lambda$. The laser-molecule electronic dipole transition operator is given as [3,26,44]

$$\mathbf{O} = \sum_{p=-1}^{1} \sum_{q=-1}^{1} (-1)^q T^1_{-p}(\boldsymbol{\varepsilon}) T^1_q(\boldsymbol{\mu}) D^1_{p,q}(\alpha\beta\gamma), \quad (1)$$

where $T^1_{-p}(\boldsymbol{\varepsilon})$ and $T^1_q(\boldsymbol{\mu})$ are the tensor operators for the electric field $\boldsymbol{\varepsilon}$ and dipole moment $\boldsymbol{\mu}$ in the space-fixed frame and molecular frame, respectively, and the wigner-D function $D^1_{p,q}(\alpha\beta\gamma)$ transforms the dipole moment from molecular frame into space-fixed frame [see Fig. 1(a)]. $T^1_{q=0}(\boldsymbol{\mu})$ triggers the parallel transition with the electronic transition dipole moment $\mu^{\Lambda}_{\parallel} = \langle\Lambda|T^1_{q=0}(\boldsymbol{\mu})|\Lambda\rangle$, while $T^1_{q=\pm1}(\boldsymbol{\mu})$ gives rise to the perpendicular electronic transition as $\Delta\Lambda = \pm1$, and the corresponding electronic transition dipole moment $\mu_{\perp} = \langle\Lambda \pm 1|T^1_{q=\pm1}(\boldsymbol{\mu})|\Lambda\rangle$.

Following Eq. (1), when studying the $X^1\Sigma \to A^1\Pi$ resonant transitions in the CO molecules, the $\Pi_{\pm\Lambda}$ states can be clearly identified and the nuclear Hamiltonian can be written in three-by-three matrix form

$$\begin{aligned}
&\mathbf{H}(q, \alpha, \beta, \gamma, \mathrm{t}) \\
&= [T_\nu + T_{\boldsymbol{R}}] + \begin{pmatrix} V_\Sigma & 0 & 0 \\ 0 & V_\Pi^{+\Lambda} & 0 \\ 0 & 0 & V_\Pi^{-\Lambda} \end{pmatrix} \\
&\quad - \mathrm{g(t)} \cos\omega\mathrm{t} \begin{pmatrix} \mu^{\Sigma}_{\parallel}\kappa_{\parallel} & \mu_{\perp}(\kappa^{+}_{\perp})^{\dagger} & \mu_{\perp}(\kappa^{-}_{\perp})^{\dagger} \\ \mu_{\perp}\kappa^{+}_{\perp} & \mu^{\Pi}_{\parallel}\kappa_{\parallel} & 0 \\ \mu_{\perp}\kappa^{-}_{\perp} & 0 & \mu^{\Pi}_{\parallel}\kappa_{\parallel} \end{pmatrix}, \quad (2)
\end{aligned}$$

where q is the internuclear distance, the first term is the vibrational and rotational kinetic energy operator, V_Σ and $V_\Pi^{\pm\Lambda} = V_\Pi$ are the potential energy curves for states $X^1\Sigma$ and $A^1\Pi_{\pm\Lambda}$, respectively [see Fig. 1(b)]. In the case of a LP pulse ($p = 0$, with laser polarization along the Z-axis), the angular transition operators $\kappa_{\parallel} = \cos\beta$ and $\kappa^{\pm}_{\perp} = \mp\frac{\sin\beta}{\sqrt{2}} e^{\mp i\gamma}$; and in a right CP pulse ($p = +1$, with laser propagation along the Z-axis), $\kappa_{\parallel} = -\frac{\sin\beta}{\sqrt{2}} e^{-i\alpha}$, $\kappa^{+}_{\perp} = -\cos^2\frac{\beta}{2} e^{-i\alpha-i\gamma}$ and $\kappa^{-}_{\perp} = -\sin^2\frac{\beta}{2} e^{-i\alpha+i\gamma}$. Equation (2) not only considers the effect of the additional angle γ related to the molecular axis and the resulting coupling between electronic orbital and nuclear rotational angular momentum, but also explicitly includes the doubly degenerate $\pm\Lambda$ states. Equation (2) could be the first time being introduced in intense laser-molecule interactions. This full theoretical description is referred to as the "Λ-4D" in the following, indicating that the four degrees of freedom $(q, \alpha, \beta, \gamma)$ and the doubly degenerate $\pm\Lambda$ states are involved in the scheme description.

Examining the elements of angular transition matrix $\Theta^{+}_{J',JM\Omega} = \langle J', M', \Omega + 1|\kappa^{+}_{\perp}|J, M, \Omega\rangle$ and $\Theta^{-}_{J',JM\Omega}$

$= \langle J', M', \Omega - 1|\kappa_\perp^-|J, M, \Omega\rangle$, pertaining to $+\Lambda$ and $-\Lambda$ states of Eq. (2), respectively, reveals that they have the same transition strengths. This suggests that both the $+\Lambda$ and $-\Lambda$ states can be excited with equal efficiency in the one-photon transition. Our recent theoretical studies of interaction with LP pulses [26–28,30,31] accounted only for the single $+\Lambda$ branch, considering the upper-left two-by-two matrix elements in Eq. (2) and using $\mu_\perp \to \sqrt{2}\,\mu_\perp$ to complement the excitation strength. In the following, this simulation strategy is referred to as "4D" scheme.

Furthermore, the usual treatment in most studies [21,32,36–38] has also ignored Λ and γ, and thus the angular transition operators for the linearly ($p = 0$) and circularly ($p = \pm 1$) polarized fields become $\kappa_\parallel = \cos\beta$, $\kappa_\perp = \sin\beta$ and $\kappa_\parallel = \sin\beta e^{\mp i\alpha}$, $\kappa_\perp = \cos\beta e^{\mp i\alpha}$, respectively. [39–41] In such a case, the rotational wave function can be simplified as $|J, M, \Omega = 0\rangle = \frac{1}{\sqrt{2\pi}} Y_J^{M^*}(\beta\alpha)$. We label this treatment as the "3D" scheme.

The simulations are performed using the multiconfigurational time-dependent Hartree method (MCTDH) [45] as implemented in the Heidelberg package. [46] The resonant laser pulse with a sin-squared envelope $\sin^2(\frac{\pi t}{T})$ is used. The vibrational degrees of freedom are described by 291 sin-DVRs (discrete variable representations) equally distributed in the region [1.0, 20.0]. The rotational basis functions are described by the L_2-normalized Wigner-D functions, with 51 exp-DVRs for β and 11 exp-DVRs for α and γ. The number of single particle functions for both degrees of freedom on the three electronic states is 10.

3. Results and Discussions. To illustrate the role of the doubly degenerate $\pm\Lambda$ states, we conducted simulations for the population dynamics in the $X^1\Sigma \to A^1\Pi$ resonant transition of a CO molecule. The required potential energy curves and transition dipole moment are taken from Refs. [42,43]. The simulations were initiated by $T = 40$ fs sin-squared LP and right CP laser pulses with a resonant frequency of $\omega = 8.55$ eV. We employed three theoretical schemes, namely "Λ-4D", "4D", and "3D", as described in the previous section. Figure 2 illustrates the total population of the ground state as a function of electric field intensity, where the left and right panels correspond to the excitation by LP and CP pulses, respectively, while each row describes the results of different initial rotational states J_0 ($|\nu_0 = 0\rangle|J_0, M_0, \Omega = 0\rangle$). Note that the results of the nonzero initial state J_0 have been averaged over the $2J_0+1$ states $|J_0, M_0, \Omega = 0\rangle$. With very intense pulses, state Π can strongly couple with the continuum state. Such coupling would deplete the populations, but it can also be included in the calculations. [33] However, with the current less intense pulse, we expect that this effect may not be significant and may not impact the observed physical phenomena. [19–28,30,31]

For the LP case [Figs. 2(a)–2(c)], all three theoretical schemes predict the same result for initial rotational states $J_0 = 0$, while there are slight differences between the 4D and 3D schemes for initial rotational states $J_0 = 1, 2$.

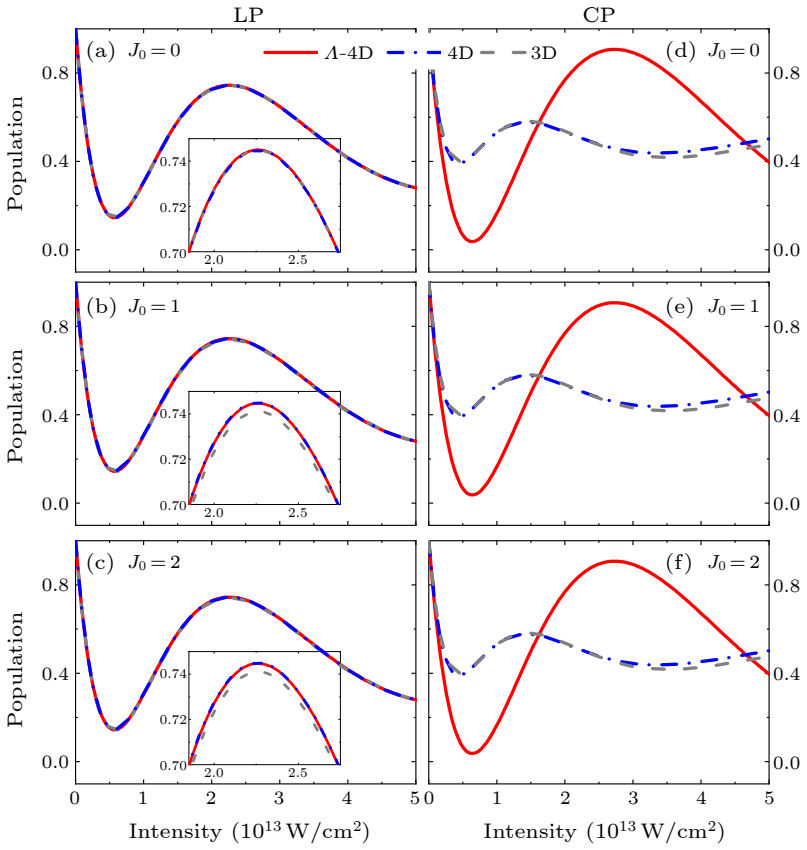

Fig. 2. The total population of the ground state $X^1\Sigma$ as a function of the field intensity. Left and right panels correspond to LP and right CP laser pulses, respectively. Each row corresponds to different initial rotational state $J_0 = 0, \ldots, 2$, and the line colors indicate theoretical schemes used in the simulations (see legends).

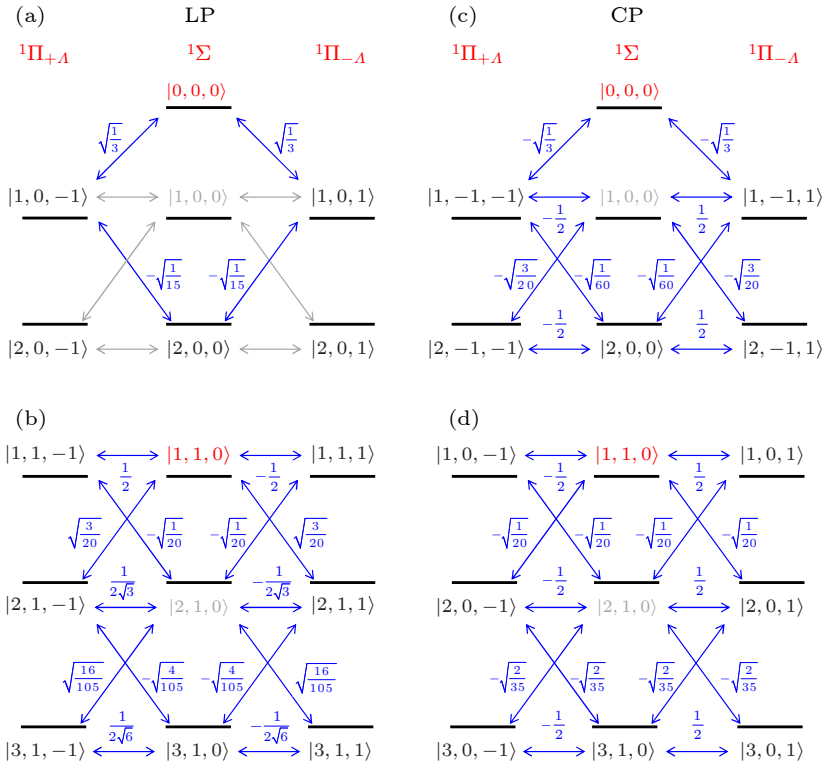

Fig. 3. Diagrams of the electron-rotational excitation channels on the $X^1\Sigma$ to $A^1\Pi_{\pm\Lambda}$ transition within the Λ-4D scheme. The left and right panels represent the LP and CP cases, respectively, while the upper and lower rows correspond to the initial rotational states $|0,0,0\rangle$ and $|1,1,0\rangle$ of carbon monoxide (marked in red), respectively. The blue arrows indicate with a number showing the amplitude of the rotational transition matrix elements $\Theta^{\pm}_{J',JM\Omega}$ between the respective rotational states.

However, there are significant differences in the populations predicted by different schemes for the CP case [Figs. 2(d)–2(f)], where the amplitude of Rabi-oscillations in the Λ-4D scheme is considerably greater than for the 4D and 3D schemes. Moreover, minor differences between the 4D and 3D schemes are also observed for laser intensities greater than $3\times10^{13}\,\mathrm{W/cm^2}$. However, the initial excited rotational states $J_0 = 1, 2$, considered here for modeling the temperature influence, show no effect compared to the case $J_0 = 0$. The differences between the 4D and 3D schemes have been analyzed in detail in our previous papers[26–28,30] and thus skipped here. In the present study, we pay primary attention to the difference in population dynamics for Λ-4D and 4D schemes, which is explained in detail below considering electron-rotational transition channels between the ground $X^1\Sigma$ and excited $A^1\Pi_{\pm\Lambda}$ states (Fig. 3).

Figure 3 depicts all the allowed rotational transitions between the $X^1\Sigma$ and $A^1\Pi_{\pm\Lambda}$ states within the full Λ-4D theoretical framework described by Eq. (2), considering both the LP (left panel) and CP (right panel) cases. The transitions are shown for the initial rotational states $|J_0, M_0, \Omega_0\rangle = |0,0,0\rangle$ (top panel) and $|1,1,0\rangle$ (bottom panel). We should note that the pathways considered in the 4D scheme include only the $+\Lambda$ branch (the left half of the diagrams). Pumped by intense pulses, the neighboring rotational states $|J_0, M_0, \Omega_0\rangle$ and $|J_2, M_0, \Omega_0\rangle$ of the ground state $X^1\Sigma$ can be excited through $|J_1, M_1, \pm\Omega_1\rangle$ of the state $A^1\Pi_{\pm\Lambda}$ within a single Rabi-cycle as $|J_0, M_0\rangle \to |J_1, M_1\rangle^{\pm} \to |J_2, M_0\rangle$ (This label will be used below to indicate the excitation channel). The corresponding nonzero angular transition strength is given by $\Theta^{J_1\pm}_{J_2,J_0M_0\Omega_0} = \Theta^{\pm}_{J_1,J_2M_0\Omega_0} \times \Theta^{\pm}_{J_1,J_0M_0\Omega_0}$. A significant feature of the Λ-4D scheme is the presence of the destructive interference between the $+\Lambda$ pathway $|J_0, M_0\rangle \to |J_1, M_1\rangle^{+} \to |J_2, M_0\rangle$ and the $-\Lambda$ pathway $|J_0, M_0\rangle \to |J_1, M_1\rangle^{-} \to |J_2, M_0\rangle$, resulting in $\Theta^{J_1+}_{J_2,J_0M_0\Omega_0} + \Theta^{J_1-}_{J_2,J_0M_0\Omega_0} = 0$ and the suppression of the population of the selected rotational state $|J_2, M_0, \Omega_0\rangle$ (shown in gray on the diagrams).

For the initial rotational state $|0,0,0\rangle$ and the LP pulse [Fig. 3(a)], the rotational wave packet in the ground state $X^1\Sigma$ does not contain odd J states due to the angular selection rule or $\Theta^{\pm}_{1,100} = 0$, and the $+\Lambda$ pathway and the $-\Lambda$ pathway yield equivalent transition strengths since $\Theta^{+1}_{2,000} = \Theta^{-1}_{2,000}$. Consequently, the Λ-4D and 4D schemes result in the same rotational excitations. This situation changes in the case of the CP pulse [Fig. 3(c)], where $\Theta^{+1}_{1,000} = -\Theta^{-1}_{1,000} \neq 0$. In this scenario, both even and odd J states contribute to the rotational excitations in the $X^1\Sigma$ state in the 4D scheme. However, in the full theoretical treatment, the state $|1,0,0\rangle$ is not excited as a result of destructive interference between the $|0,0\rangle \to |1,1\rangle^{+} \to |1,0\rangle$ and $|0,0\rangle \to |1,1\rangle^{-} \to |1,0\rangle$ channels, thus only even rotational states are populated in the ground electronic state. This discussion explains the fundamental role of doubly degenerate $\pm\Lambda$ states in the context of rotational excitations.

In the case of initial rotational state $|1,1,0\rangle$ and LP pulse [Fig. 3(b)], the state $|2,1,0\rangle$ can be excited via two channels: $|1,1\rangle \to |1,1\rangle^{\pm} \to |2,1\rangle$ and $|1,1\rangle \to |2,1\rangle^{\pm} \to |2,1\rangle$. The amplitudes of these transitions are $\Theta^{J_1+}_{J_2,J_0M_0\Omega_0} = -\Theta^{J_1-}_{J_2,J_0M_0\Omega_0}$, indicating that the rotational state $|2,1,0\rangle$ cannot be excited (marked in gray), and thus only odd rotational states can be excited within the Λ-4D scheme description. In contrast, although $\Theta^{+1}_{2,110} = -\Theta^{+2}_{2,110}$ also in the 4D scheme, channels $|1,1\rangle \to |1,1\rangle^{+} \to |2,1\rangle$ and $|1,1\rangle \to |2,1\rangle^{+} \to |2,1\rangle$ do not fully destruct each other. This is because the rovibrational wave functions for $J = 1$ and $J = 2$ in the $A^1\Pi_{\pm\Lambda}$ state exhibit minor differences, allowing for the weak excitation of the even rotational state, which is consistent with the results indicating that the 4D and Λ-4D schemes produce relatively similar results with LP pulses. The situation is similar for the CP pulse in the full theoretical description [Fig. 3(d)], while in the 4D scheme $\Theta^{+1}_{2,110} = \Theta^{+2}_{2,110}$ and the two channels $|1,1\rangle \to |1,0\rangle^{+} \to |2,1\rangle$ and $|1,1\rangle \to |2,0\rangle^{+} \to |2,1\rangle$ interfere constructively to populate the rotational state $|2,1,0\rangle$. Finally, the $-\Lambda$ branch is absent from the basis of 4D scheme, the population will be forced into higher rotational states, so the 4D scheme involves a greater number of rotational states in the excitations, which will certainly decrease the amplitude of Rabi-oscillations compared to that in the Λ-4D scheme [see Fig. 2].

Let us now analyze the excited rotational states of the ground $X^1\Sigma$ and excited $A^1\Pi$ states. For this we choose the pulse intensity $I = 2.66 \times 10^{13}\,\mathrm{W/cm^2}$, approximately corresponding to one Rabi-cycle at the end of the pulse (40 fs) within the Λ-4D scheme (see Fig. 2). Figure 4 illustrates details of the rotational wave packet dynamics initiated from the initial state $|0,0,0\rangle$ by LP (left panel) and CP (right panel) pulses. One can see that in the LP case, the Λ-4D and 4D schemes exhibit high consistency.

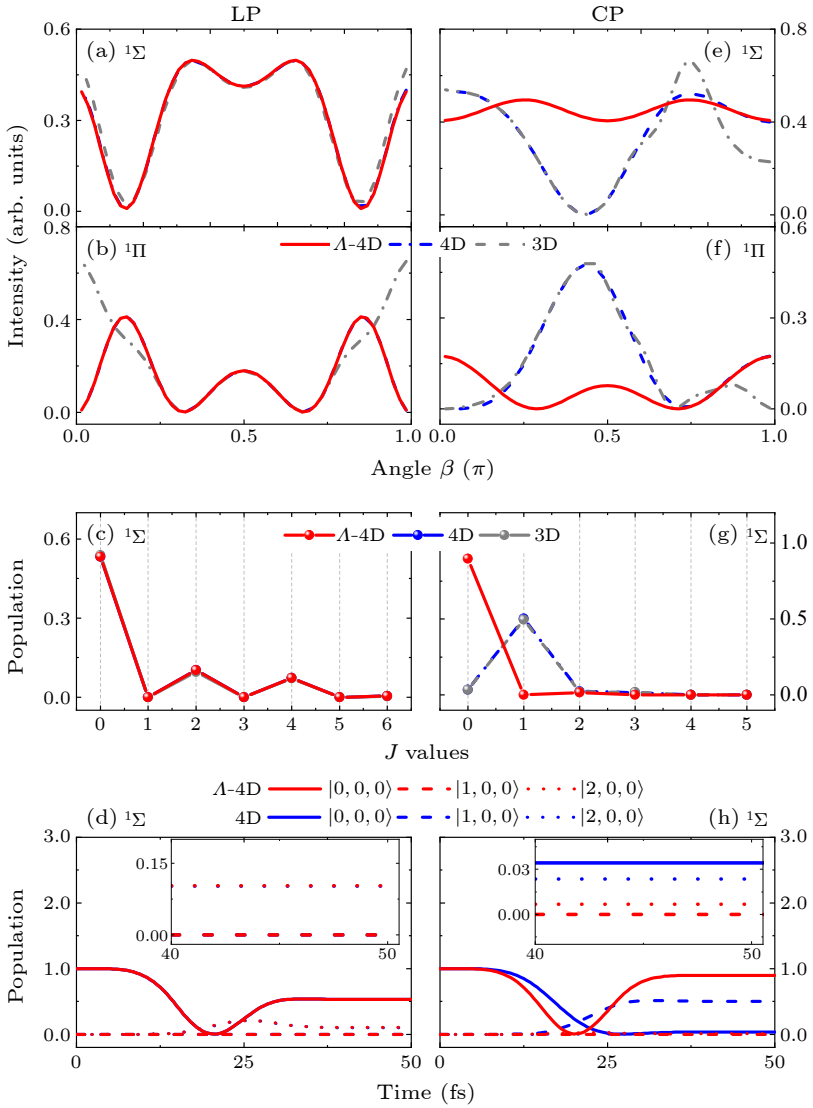

Fig. 4. Rotational wave packet for the LP (left panel) and CP (right panel) pulse excitations from the initial rotational state $|0,0,0\rangle$ and the pulse intensity $I = 2.66 \times 10^{13}\,\mathrm{W/cm^2}$. Angular distribution of the rotational wave packet in (a) and (e) the ground $X^1\Sigma$ as well as (b) and (f) excited $A^1\Pi$ states. The density of the occupied rotational states J in (c) and (g) the ground state at the end of the pulse (40 fs). (d) and (h) Population dynamics of the selected rotational states in the $X^1\Sigma$ state. Different line styles indicate theoretical models used.

The wave packet angular distributions in the ground $X^1\Sigma$ [Fig. 4(a)] and excited $A^1\Pi$ [Fig. 4(b)] states show a symmetric distribution with respect to $\beta = 0.5\pi$ for the three models, due to the identical population distributions of the rotational states in the ground state [Fig. 4(c)]. However, the simplest theoretical approach—the 3D scheme—results in significant deviations near $\beta = 0$ and π, especially in the excited state [Fig. 4(b)], as it was previously discussed in detail.[26] In the case of CP pulse excitation, the situation changes dramatically (right panel of Fig. 4). Indeed, the angular distributions in the Λ-4D scheme are symmetric with respect to $\beta = 0.5\pi$, similarly to the LP mode, since only even rotational states are populated in the ground state $X^1\Sigma$. In contrast, the limited accuracy of the 4D and 3D schemes results in the asymmetry of the profiles, since both even and odd J values are populated, as shown in the inset of Fig. 4(g). The angular distribution of the 3D scheme also deviates from the 4D simulations for $\beta > 0.6\pi$.

Figures 4(d) and 4(h) compare the time-dependent populations for the three lowest rotational components of the ground $X^1\Sigma$ state computed using the Λ-4D and 4D theoretical approaches. One can see that the Rabi-cycling dynamics are identical for both models in the case of LP pulse [Fig. 4(d)], when the $|1,0,0\rangle$ state is not excited in either scheme and the $|2,0,0\rangle$ state gains a minor population within a single Rabi-cycle. In the CP case [Fig. 4(h)], computed using the full Λ-4D scheme, population of the $|1,0,0\rangle$ state vanishes due to the destructive interference of the rotational excitation pathways, and the rotational population returns mostly to the $|0,0,0\rangle$ state after a full Rabi-cycle with a minor population transfer to the state $|2,0,0\rangle$. In contrast, within the 4D model neglecting the doubly degenerate $\pm\Lambda$ states, most of the rotational population accumulates in the $|1,0,0\rangle$ state after the pulse. This contrast demonstrates clearly the importance of explicitly considering the doubly degenerate $\pm\Lambda$ states for accurate theoretical modeling.

To account for thermal effects, we also considered excitation from the initial state $|1,1,0\rangle$, as illustrated in Fig. 5. For the angular distribution of the rotational wave packet in the case of LP excitation [Figs. 5(a) and 5(b)], only minor differences between the Λ-4D and 4D schemes are observed in the ground state [panel (a)], while there are sufficient differences at β close to 0 and π in the excited state $^1\Pi$ [panel (b)]. The angular distribution

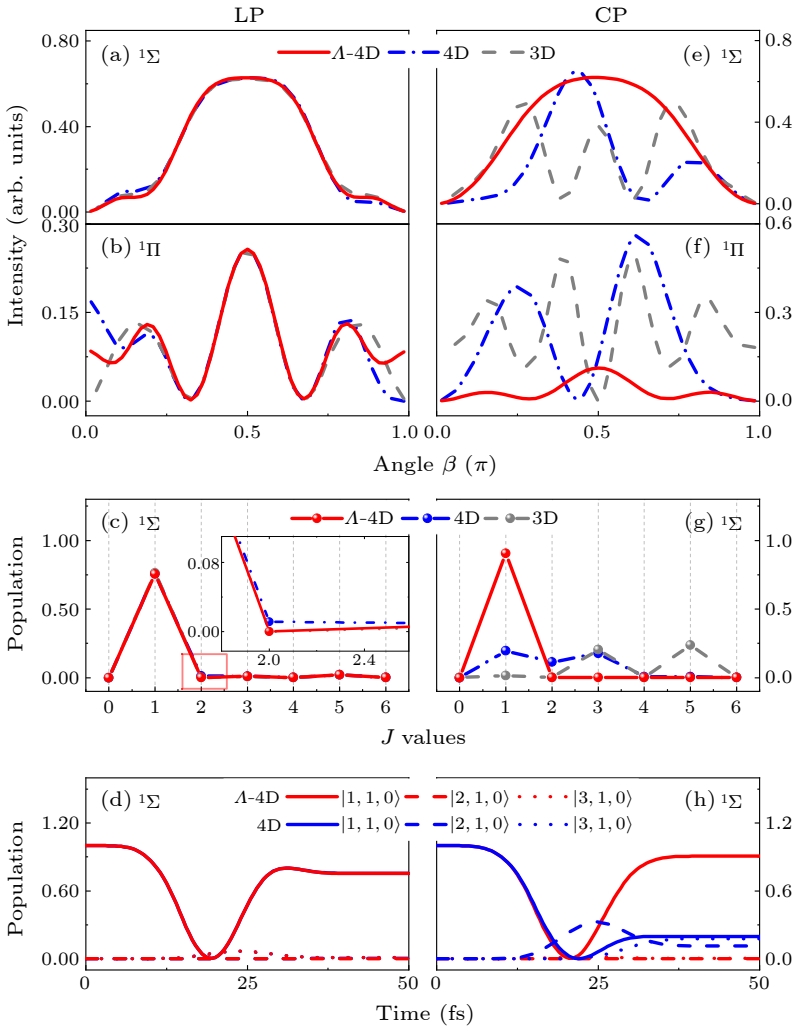

Fig. 5. Same as Fig. 4, but with the initial rotational state $|1,1,0\rangle$.

for the ground state is no longer symmetric in the 4D scheme, due to the slight excitation of the $|2,1,0\rangle$ state [see the inset in panel (c)]. For the CP case (right panel), the angular asymmetry in the 4D scheme increases dramatically [Figs. 5(e) and 5(f)], as the $|2,1,0\rangle$ state is mistakenly excited, leading to non-negligible populations in higher rotational states. Similarly to the case of initial state $J_0 = 0$, a significant difference in the Rabi dynamics of individual rotational states is also observed between the Λ-4D and 4D models [Figs. 5(d) and 5(h)], resulting from the neglect of both $\pm\Lambda$ states in the latter model.

Before concluding, we would like to make some notes regarding possible experimental observations of the discussed phenomena. Diatomic molecules with the ground Σ state and the excited bound Π state (such as CO, CH^+, and NH, among others) are good potential candidates. For the pump pulse, a CP pulse in resonance with the $\Sigma \to \Pi$ electronic transition is required, with an intensity sufficient to drive Rabi cycling of the populations (for CO, the intensity should be approximately 3.0×10^{13} W/cm^2). While thermal effects on population dynamics in relation to pulse intensity may not be significant, it is still preferred to use cold targets. Any measurements or probe signals sensitive to electronic populations could be proposed for observation.

When considering the transition between doublet states $^2\Sigma \to {}^2\Pi$, the tiny spin-rotation coupling breaks the degeneracy of the $\pm\Lambda$ states and introduces the phenomenon of Λ-doubling. At the same time, as the $+\Lambda$ and $-\Lambda$ states become weakly coupled, the molecular wavefunction can be rewritten as an appropriate linear combination of the Hund's case (a) wavefunctions of the $\pm\Lambda$ states, in the spirit of the Wang transformation.[2] This treatment resembles a change in representation from the adiabatic to the diabatic framework. In this context, $p^{\pm}$ must be introduced to denote the sign or parity of the linearly combined basis or wavefunction; more details can be found in Refs. [1–3].

Returning to the present transition between singlet states $^1\Sigma \to {}^1\Pi$, the $\pm\Lambda$ states are degenerate and decoupled. In addition to the current adiabatic strategy, as expressed in Eq. (2), which explicitly considers the $\pm\Lambda$ states using non-combined wavefunctions, we can also adopt an equivalent diabatic strategy using combined wavefunctions. In this case, the diabatic state is identified by $p^{\pm}$ rather than $\pm\Lambda$ states. Consequently, equation (2) reduces to a two-by-two matrix based on parity selection, with the transition matrix elements redefined using the combined basis. The destructive channels presented in Fig. 3 actually reflect the parity of the combined states $+\Lambda$ and $-\Lambda$. Anyway, both adiabatic and diabatic strategies emphasize the importance of considering "near"-degenerate states during intense pulse excitations.

We should also note that in excitations by off-resonant pulses with significant detuning, or in the case of multiphoton excitation with IR pulses, much more intense laser pulses are required to achieve Rabi oscillations between electronic states. In these situations, nonlinear effects may also play a role and could even dominate the dynamics. Further studies are needed in the future to unveil the interplay between nonlinear dynamics and near-degenerate states.

4. Conclusion. We theoretically investigated the impact of doubly degenerate $\pm\Lambda$-states on the rotational excitations, resonantly driven by an intense laser pulse in the $X^1\Sigma \to A^1\Pi$ transition showcased in the CO molecule. The results show that explicitly including $\pm\Lambda$ states significantly influences the rotational population in an intense laser field, particularly in the case of CP light. We found that the presence of doubly degenerate $\pm\Lambda$ states coherently suppresses certain electron-rotational transition channels between the $\Pi_{\pm\Lambda}$ and Σ states during electronic Rabi-cycling, thus significantly altering the rotational wave packet dynamics in the ground state $^1\Sigma$. Our findings highlight the importance of considering the doubly degenerate $\pm\Lambda$ states in theoretical modeling of intense laser-molecule interactions for accurate prediction of complex electron-rotational excitation processes. The observed phenomena provide valuable theoretical support and practical guidance for a deeper understanding of quantum system dynamics and precise control in strong-field and ultrafast sciences. Moreover, this work raises general questions about the roles of near-degenerate states in intense laser-matter interactions. Sometimes, it is acceptable to treat these states as one state, while at other times this approach may not be accurate. Further research is needed to investigate different scenarios under intense laser pulses.

Acknowledgments. We thank O. Vendrell and J.M. Rost for helpful discussions. This work was supported by the National Natural Science Foundation of China (Grant No. 12374238), the Postdoctoral Science Foundation of Shaanxi Province (Grant No. 2024BSHSDZZ148), and Ministry of Science and Higher Education of Russian Federation (Grant No. FSRZ 2023-0006).

References

[1] Herzberg G 1950 *Molecular spectra and molecular structure* **1**: Spectra of diatomic molecules (D. Van Nostrand)
[2] Zare R N 1988 *Angular Momentum: Understanding Spatial Aspects in Chemistry and Physics* (John Wiley & Sons, New York)
[3] Lefebvre-Brion H and Field R W 2004 *The Spectra and Dynamics of Diatomic Molecules: Revised and Enlarged Edition* (Elsevier)
[4] Emma P, Akre R, Arthur J *et al.* 2010 *Nat. Photon.* **4** 641
[5] Spielmann C, Burnett N. H, Sartania S *et al.* 1997 *Science* **278** 661
[6] Zhao K, Zhang Q, Chini M, Wu Y, Wang X, and Chang Z 2012 *Opt. Lett.* **37** 3891
[7] Allaria E, Appio R, Badano L *et al.* 2012 *Nat. Photon.* **6** 699
[8] Harmand M, Coffee R, Bionta M R *et al.* 2013 *Nat. Photon.* **7** 215
[9] Pellegrini C, Marinelli A, and Reiche S 2016 *Rev. Mod. Phys.* **88** 015006
[10] Bostedt C, Boutet S, Fritz D M *et al.* 2016 *Rev. Mod. Phys.* **88** 015007

[11] Kraus P M, Zürch M, Cushing S K, Neumark D M, and Leone S R 2018 *Nat. Rev. Chem.* **2** 82
[12] Dong X X, Liu Y R, Kimberg V, Vendrell O, Wu Y, Wang J G, Chen J, and Zhang S B 2022 *Commun. Phys.* **5** 181
[13] Rolles D 2023 *Adv. Phys. X* **8** 2132182
[14] Chergui M, Beye M, Mukamel S, Svetina C, and Masciovecchio C 2023 *Nat. Rev. Phys.* **5** 578
[15] Dong X X, Gong M, Zhao X, Liu Y R, Cheng Y, Wu Y, Wang J G, Chen J, and Zhang S B 2024 *New J. Phys.* **26** 013050
[16] Liu Y R, Bai X, Nan Q W, Kimberg V, Gong M, Yang Y K, Cheng Y, Chen J, Vendrell O, Ueda K, Rost J M, and Zhang S B 2025 *Commun. Phys.* **8** 331
[17] Moiseyev N, Šindelka M, and Cederbaum L S 2008 *J. Phys. B* **41** 221001
[18] Šindelka M, Moiseyev N, and Cederbaum L S 2011 *J. Phys. B* **44** 045603
[19] Halász G J, Šindelka M, Moiseyev N, Cederbaum L S, and Vibók A 2012 *J. Phys. Chem. A* **116** 2636
[20] Demekhin P V and Cederbaum L S 2013 *J. Chem. Phys.* **139** 154314
[21] Corrales M E, González-Vázquez J, Balerdi G, Solá I R, de Nalda R, and Bañares L 2014 *Nat. Chem.* **6** 785
[22] Stapelfeldt H and Seideman T 2003 *Rev. Mod. Phys.* **75** 543
[23] Halász G J, Vibók A, and Cederbaum L S 2015 *J. Phys. Chem. Lett.* **6** 348
[24] Halász G. J, Vibók A, Meyer H D, and Cederbaum L S 2013 *J. Phys. Chem. A* **117** 8528
[25] Triana J F and Sanz-Vicario J L 2019 *Phys. Rev. Lett.* **122** 063603
[26] Liu Y R, Wu Y, Wang J G, Vendrell O, Kimberg V, and Zhang S B 2020 *Phys. Rev. A* **102** 033114
[27] Liu Y R, Wu Y, Wang J G, Vendrell O, Kimberg V, and Zhang S B 2020 *Phys. Rev. Res.* **2** 043348
[28] Liu Y R, Kimberg V, Wu Y, Wang J G, Vendrell O, and Zhang S B 2021 *J. Phys. Chem. Lett.* **12** 5534
[29] Zhu Y P, Liu Y R, Zhao X, Kimberg V, and Zhang S B 2021 *Chin. Phys. Lett.* **38** 053201
[30] Liu Y R, Kimberg V, Wu Y, Wang J G, Vendrell O, and Zhang S B 2022 *Phys. Rev. Res.* **4** 013066
[31] Liu Y R, Kimberg V, Gong M, Cheng Y, Wu Y, Wang J G, and Zhang S B 2025 *Phys. Rev. A* **111** 013122
[32] Cederbaum L S, Chiang Y C, Demekhin P V, and Moiseyev N 2011 *Phys. Rev. Lett.* **106** 123001
[33] Demekhin P V, Chiang Y C, and Cederbaum L S 2011 *Phys. Rev. A* **84** 033417
[34] Nan Q W, Wang C, Yu X Y, Zhao X, Cheng Y, Gong M, Liu X J, Kimberg V, and Zhang S B 2023 *Chin. Phys. Lett.* **40** 093201
[35] Nan Q W, Kimberg V, Wang C, Gong M, Cheng Y, Ueda K, and Zhang S B 2025 *J. Phys. Chem. Lett.* **16** 9561
[36] Puschnig P, Boese A D, Willenbockel M *et al.* 2017 *J. Phys. Chem. Lett.* **8** 208
[37] Triana J F and Sanz-Vicario J L 2019 *Phys. Rev. Lett.* **122** 063603
[38] Tóth A, Csehi A, Halász G J, and Vibók A 2020 *Phys. Rev. Res.* **2** 013338
[39] Halász G J, Csehi A, Vibók A, and Cederbaum L S 2014 *J. Phys. Chem. A* **118** 11908
[40] Kim J H, Liu W K, McCourt F R W, and Yuan J M 2000 *J. Phys. Chem.* **112** 1757
[41] Carrasco S, Rogan J, Valdivia J A, Chang B Y, Malinovsky V S, and Sola I R 2022 *Phys. Chem. Chem. Phys.* **24** 2966
[42] Cooper D L and Kirby K 1987 *J. Chem. Phys.* **87** 424
[43] Borges I, Caridade P, and Varandas A 2001 *J. Mol. Spectrosc.* **209** 24
[44] Whiting E E and Nicholls R W 1974 *Astrophys. J. Suppl. Ser.* **27** 1
[45] Beck M, Jäckle A, Worth G, and Meyer H D 2000 *Phys. Rep.* **324** 1
[46] Worth G A, Beck M H, Jäckle A, and Meyer H D 2000 The MCTDH Package, Version 8.2. Meyer H D 2002 Version 8.3. Meyer H D 2007 Version 8.4. Vendrell O and Meyer H D 2013 Version 8.5. Versions 8.5 and 8.6 contain the ML-MCTDH algorithm. Current version(2024): 8.6.7. See http://mctdh.uni-hd.de for a description of the Heidelberg MCTDH package.